THE JOURNAL OF PHYSICAL CHEMISTRY B

Article

pubs.acs.org/JPCB

Cytochrome P450-Catalyzed Degradation of Nicotine: Fundamental Parameters Determining Hydroxylation by Cytochrome P450 2A6 at the 5′-Carbon or the *N*-Methyl Carbon

Renata A. Kwiecień,*[,†] Jean-Yves Le Questel,[†] Jacques Lebreton,[†] Marcel Delaforge,[‡] François André,[‡] Emilie Pihan,[‡] Anaïs Roussel,[‡] Anaïs Fournial,[†] Piotr Paneth,[§] and Richard J. Robins*[,†]

[†]Laboratory for the Study of Biosynthesis by Isotopic Spectroscopy, Interdisciplinary Chemistry: Synthesis, Analysis and Modeling (CEISAM), UMR6230, University of Nantes-CNRS, 2 rue de la Houssinière, BP 92208, F-44322 Nantes 3, France

[‡]Laboratoire Stress Oxydant et Détoxication, CNRS UMR8221, iBiTec-S/SB2SM, CEA Saclay, 91191 Saclay, France

[§]Laboratory for Isotope Effects Studies, Faculty of Chemistry, Institute of Applied Radiation Chemistry, University of Technology Lodz, Zeromskiego 116, 90-924 Łodź, Poland

Supporting Information

ABSTRACT: The oxidation of (2′*S*)-nicotine in the active site of human cytochrome P450 2A6 has been subjected to a detailed analysis by theoretical quantum mechanical/molecular mechanical (QM/MM) calculations linked with a theoretical and experimental study of the associated isotope effects. The study has focused on seeking an explanation as to why oxidation at the 5′-carbon position (A) is favored over oxidation at the methyl carbon (C_{Me}) position (B). It is deduced that the choice of hydrogen for abstraction is not determined by geometric features of the active site, but by the lower energy barrier associated with 5′ oxidation. N-Demethylation leading to *N*-hydroxymethylnornicotine requires ca. 6.5 kcal/mol more energy to transfer a hydrogen atom than is required for oxidation on the carbon 5′. Neither protonation of the pyrrolidine nitrogen (N1′) nor inclusion of a water molecule in the reaction process influences the balance between the two oxidation pathways. In both cases, the hydrogen transfer step is rate limiting. An analysis of the calculated kinetic isotope effects indicates that the presence of a ^{2}H in either the C5′ or the C_{Me} positions has a significant effect on the reaction kinetics. However, the experimental values of around 2.2−2.6 are considerably lower than those predicted by theoretical calculations (9.3 and 6.9 for C5′ or the C_{Me} positions, respectively, in the LS state of Cpd I), typical of the masking commonly found for CYP450 reactions. The fact that similar values are found for cotinine formation from both substrates, however, may indicate that the measured value is not that for H-abstraction but, rather, is a combined value for ^{2}H influence on electronic redistribution between iminium states of the pyrrolidine ring. This is the first time that oxidation at the C5′ or the C_{Me} positions has been directly compared and that isotope effects have been obtained for this reaction in a human cytochrome P450 reaction.

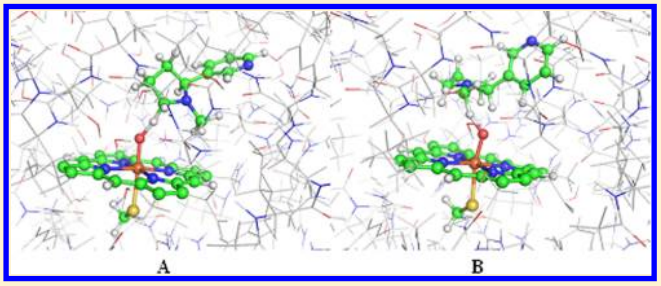

INTRODUCTION

The subtlety of the architecture of the active sites of enzymes continues to be a subject of endless fascination, particularly when it comes to defining how selectivity and reactivity are determined. Though some enzymes display a very narrow range of catalytic functions, others show a broad substrate range. Such knowledge is of value in understanding how bioactive molecules are metabolized and in designing better and more stable compounds for pharmaceutical applications. A group of enzymes of paramount importance in this respect is the cytochrome P450 monooxygenases (CYP450s), which display an extraordinary versatility in their substrate range.[1,2] Considerable advances have been made in understanding the architectural features that define why certain groups of substrates are metabolized by some classes of CYP450 but not by others.[3,4] However, a further complexity is that closely related CYP450s will metabolize the same substrate to more than one product: indeed with some substrates the same CYP450 can metabolize a compound in more than one manner.

This is the case with the CYP450-dependent metabolism of (2′*S*)-nicotine (**1**) (Chart 1), the highly toxic natural product in tobacco primarily responsible for addiction.[5] The major site of action of nicotine is brain tissue, where its interaction with nicotinic acetylcholine receptors can lead to a pleasurable sensation. Its toxicity is modulated by rapid detoxification by a number of different CYP450s of the CYP2 superfamily, major catalysts for the phase 1 metabolism of xenobiotics.[6]

In humans, the primary excretory product of detoxification is cotinine (**5**) (70−80%),[7] produced by oxidation by CYP2A6 or CYP2A13 of the C5′ position to yield 5′-hydroxynicotine (**4**),

Received: May 3, 2012
Revised: June 5, 2012
Published: June 7, 2012

dx.doi.org/10.1021/jp304276v | *J. Phys. Chem. B* 2012, 116, 7827−7840

Chart 1. Structures of (2′*S*)-Nicotine (1), (2′*S*)-*N*-Hydroxymethylnornicotine (2), (2′*S*)-Nornicotine (3), (2′*S*)-5′-Hydroxynicotine (4), and (2′*S*)-Cotinine (5)

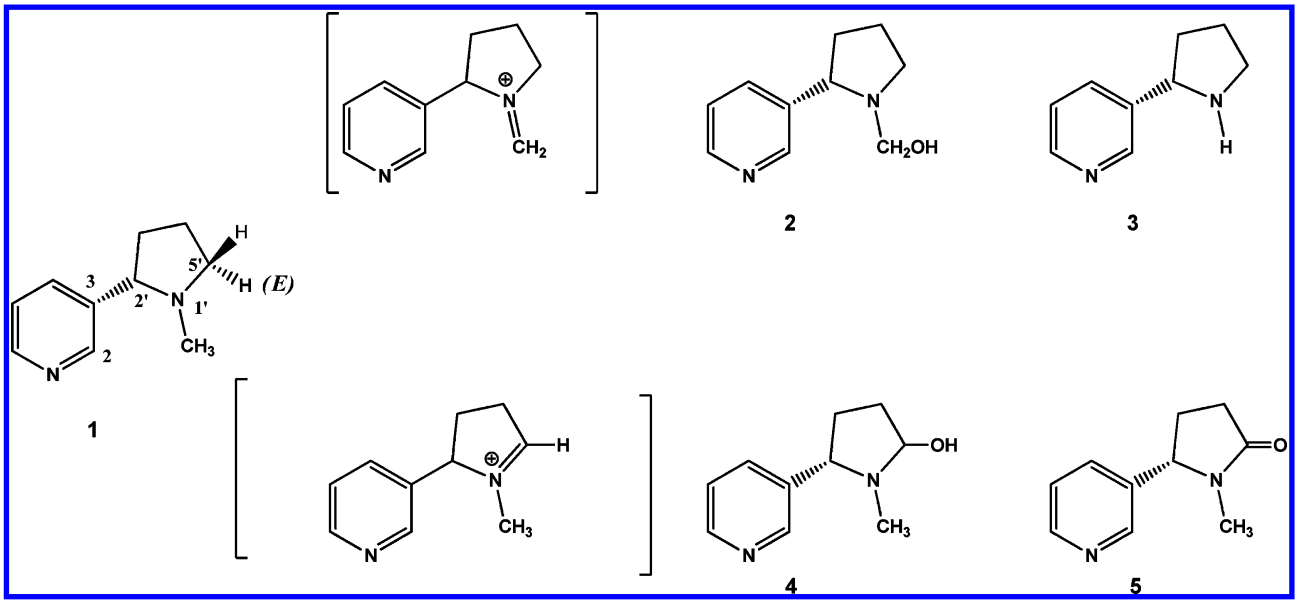

which is then oxidized by soluble aldehyde oxidase. As an alternative, nicotine is N-demethylated to nornicotine (**3**), a reaction catalyzed by the same CYP450s.[8,9] Although only 2−3% of inhaled nicotine is excreted in humans as nornicotine,[10,11] there is good evidence to consider that this reaction is more significant than apparent from its urinary levels. CYP2A6 is primarily located in hepatic tissue,[12,13] whereas CYP2A13 is found in a wide range of tissues, including nasal mucosa, trachea, lung, and brain.[14,15] Although in liver CYP2A6 is only expressed at moderate levels, liver has a large metabolic capacity,[16] so CYP2A6-derived urinary metabolites predominate over CYP2A13-derived metabolites. However, in vivo studies on animals have shown that nornicotine is present in brain at significant levels: ca. 20% of the total amount of nicotine and its metabolites[17−19] and up to a concentration equivalent to that of nicotine.[20] It is thus clear that nornicotine is a major metabolite in brain. Furthermore, the half-life of nornicotine in human plasma and rat brain are respectively 6-fold and 3-fold longer than that of nicotine.[10,21] This is of considerable importance, because nornicotine is metabolized to the carcinogen, *N*′-nitrosonornicotine. It should also be noted that nornicotine is the principal product of nicotine degradation in plants, due largely to the activity of CYP82E4.[22]

Such observations lead to two intriguing questions. The first is "What reaction parameters influence the relative levels of C5′-hydroxylation and N-demethylation in a given P450 active site?". The second is "What features of the architecture of the active sites of two CYP450s determine the relative levels of 5′-hydroxylation and N-demethylation?". Although several attempts to resolve these questions have been made over the years, no clear-cut answers have yet been advanced. This is in part due to the difficulties inherent in both experimental and theoretical studies of CYP450 reactions. The first reported study addressing these questions for nicotine is that of Jones et al.[23] who measured differences in binding energies of (*S*)- and (*R*)-nicotine and related the observed energy differences to variations of orientation of the two enantiomers in the active site of the bacterial enzyme CYP101 obtained by molecular dynamics calculations. The binding configurations for both enantiomers placed the *trans*-5′-H closer to the O−Fe than the *N*-methyl, orientations compatible with an experimentally determined preference for oxidation at the C5′ position. Furthermore, CYP101 is characterized by a flexible active site that makes it relatively promiscuous in its reactivity,[24] in contrast to the human CYP2A6 and CYP2A13, which have narrow active site cavities.[14] Thus, although this study pioneered the way to probing architecture/reactivity in these oxidations of nicotine, it remained open to what extent reaction mechanism rather than architecture might favor one oxidation reaction over the other.

Clearly architecture must play a role: the active site must both be accessible and possess a geometry that permits a suitable orientation. Very similar amino acids are involved in substrate binding in CYP2A6 and CYP2A13,[14] yet their metabolic profile for nicotine oxidation differs. Flexibility around the active site coupled with allosteric effects makes prediction difficult based on static structural analysis alone.[4] Indeed, movements within the structure are frequently required for channel opening, both for substrate entry and for product release.[25] The role of such architectural flexibility has been highlighted in a recent in silico study of the plant enzymes CYP82E4 and CYP82E3, where it was shown that mutation of an amino-acid residue distal to the active site should block or induce nicotine N-demethylase activity.[26,27]

However, to establish those parameters that regulate reactivity, the reaction pathway must be elucidated. A classical approach to probing reaction mechanism is the study of associated isotope effects. For CYP450-catalyzed N-demethylation, the overall evidence is that the ^{2}H heavy isotope effect is associated with C−H bond fission, typical experimental values falling within the range 2.0−3.5.[28−30] When the reaction coordinate was calculated for the first time for nicotine metabolism using a small model semi ab initio method (SAM1), it was concluded that the oxygen rebound step was rate-controlling on the basis of the correlation between experimentally determined ^{2}H and ^{15}N heavy isotope effects and those calculated using this model.[31] However, although this was the first time that the reaction coordinate was obtained for nicotine demethylation, the influence of neither the protein environment nor the charge state of nicotine was taken into consideration.

The question of the reaction coordinates has been revisited within the frame of density functional theory (DFT) using a

dx.doi.org/10.1021/jp304276v | *J. Phys. Chem. B* 2012, 116, 7827−7840

QM model to probe the selectivity of the reaction between H abstraction from the methyl group or from the C5′ position.[32] On the basis that at physiological pH (7.4) nicotine is about 80% protonated in solution (pK_a = 7.8), this study considered only the protonated species of the amine nitrogen. This choice was contrary to the majority of studies of the reaction chemistry of amine metabolism by P450s.[2,33] Under these conditions, a distinct reaction pathway leading to each product was described, in both low-spin (LS) and high-spin (HS) states. Reaction in the HS state was found to be energetically favored and C5′-H abstraction was privileged over C_{Me}-H abstraction, but only by ca. 3 kcal/mol (22.2 versus 24.9 in the HS, 23.5 versus 26.6 in the LS). A small barrier for the rebound step of about 3−4 kcal/mol was also found. Though these calculations clearly indicated C5′-H abstraction to be energetically favored, a difficulty with this model is the need to "deprotonate" *N*-hydroxymethylnornicotine for the C−N bond to rupture.

Having established the predominant reaction as being C5′-H abstraction, this process was recently probed in depth by the same authors through a detailed QM/MM analysis of H abstraction from the C5′ position in the reaction center of CYP2A6.[34] Thus, the enzymatic environment was accounted for in the overall reaction scheme. The authors claimed to provide theoretical evidence that the dominant molecular species of (2′*S*)-nicotine in the CYP2A6 active site exists in the free-base state. Following a comprehensive study of the possible orientations of nicotine in the active site, and of the energy barriers involved in H-abstraction and OH rebound, they demonstrated for the neutral substrate (i) that the LS state gives lower reaction barriers (in contrast to the QM results previously obtained with protonated nicotine), (ii) that, in terms of the energetics, the reaction does not favor the *trans*-5′-H over the *cis*-5′-H for H abstraction (14.1 and 14.4 kcal/mol, respectively), and (iii) that the energy barrier in the CYP2A6 environment is lower than that in the QM small model. By determining the binding energies, they also elegantly revealed that the major factor determining the choice of H for ablation was binding energy, rather than bond-breaking energy. Thus, they showed a good correlation between the theoretical stereoselectivity of the CYP2A6 catalyzed (*S*)-nicotine 5′-hydroxylation, that is to say, the product distribution of *trans*-5′-hydroxynicotine and *cis*-5′-hydroxynicotine and the ratio obtained experimentally.[35,36]

Despite the major advances in the understanding of the catalytic mechanism of CYP450 for nicotine 5′-hydroxylation due to this recent study,[34] the picture is far from complete and a number of crucial questions remain unanswered. How do the energetics of C5′ and C_{Me} oxidation compare in the active site of CYP2A6? What is the effect of N1′ protonation of nicotine? Indeed, can we be sure that neutral nicotine is the preferred form, given that both chemical forms have not been considered in the QM/MM studies? Is there any role of a molecule of catalytic water in the overall reaction process? (It must be born in mind that the cleavage of the C−N bond in demethylation is a heterolytic hydrolysis.)

To provide answers to these questions, we have carried out a systematic in-depth study of those parameters primarily determinant of reactivity within the active site by a hybrid QM/MM integrated analysis through the ONIOM methodology (B3LYP:Amber). Thus it is possible to compare directly results from all the calculations performed. The decision to use the B3LYP functional is based on its previous history of exploitation in the field of the study of CYP450 reactivity,[2] and recent studies indicating it to provide realistic spin-state energies in quantum chemical studies of metalloenzymes.[37,38] We have also chosen a higher resolution PDB structure of CYP2A6 than previously exploited. In addition, an analysis of associated isotope effects, as a means to assess the reaction pathways from both a theoretical and an experimental perspective, has been carried out.

METHODS

Preparation of Protein Structures. A crystal structure of human CYP450, isoform 2A6, in complex with the inhibitor *N*-methyl(5-(pyridin-3-yl)furan-2-yl)methanamine (D2G) deposited in the Protein Data Bank (PDB: 2FDV)[39] was selected on the basis of its high resolution (1.65 Å) and the size and position of the inhibitor that was used during the preparation process. Only subunit A was used. This choice is justified by the best B-factors of this subunit (visualized in SwissPDB viewer: www.expasy.org/spdbv).[40] The structure includes 3803 heavy atoms (protein and heme), 411 crystallographic water molecules, and 10 atoms of inhibitor.

The structure of PDB:2FDV was manually modified so that the active site contained compound I: CYP450 O═Fe(IV) state (Cpd I). The two carbon atoms of D2G ligated to the Fe-bound nitrogen were removed and nitrogen was replaced by oxygen (Figure SI1, Supporting Information). The 2-(3-pyridyl)furan part of D2G was kept intact. The protonation state of histidine residues was determined on the basis of results obtained from the MolProbity Server.[41,42] After visual inspection of the structure in SwissPDB viewer, the protonation state was finally assigned as: Nδ HIS: 72, 84, 229, 254, 357, 415, 477 and Nε HIS: 320, 328. Amber force field parameters for heme were taken from Rydberg et al.[43]

Preparation of Nicotine Structures. The geometry of neutral (2′*S*)-nicotine used for the preparation of missing parameters for the Amber03 force field was taken from our previous study,[31] and that of the protonated (2′*S*,1′*R*)-nicotine·H^+ species was obtained by manually adding a proton to (2′*S*)-nicotine. Geometries of nicotine (neutral and protonated) were reoptimized at the B3LYP/6-31G(d) level using the Gaussian03 program.[44] RESP[45] point charges were calculated at the B3LYP/cc-pVTZ//HF/6-31G(d,p) level using the Gaussian03 program.[44] The same level of theory was applied to minimize the geometry of the 2-(3-pyridyl)furan and to calculate the corresponding RESP charges. The Antechamber[46] module of Amber 9[47] was used to generate the parameter and topology files for all three ligands.

Molecular Dynamics and Molecular Dockings. *Molecular Dynamics Preparation of Structure for Nicotine Docking.* The model of CYP2A6 with Cpd I and 2-(3-pyridyl)furan was relaxed during a short molecular dynamics (MD) run as a preparation step for docking.[48] To overcome the limitation of the ArgusLab4.0.1 software docking program, which considers the active site as rigid, protein was relaxed prior to docking by performing 0.5 ns MD runs on the modified PDB structure with 2-(3-pyridyl)furan. This ligand has a volume similar to that of nicotine, thus ensuring that the active site volume is large enough to fit the reactant.

Crystallographic water molecules were kept in their initial positions and the whole model was solvated in an octahedron periodic box. The distance between the box walls and the protein was set to 9.0 Å, which resulted in the inclusion of ca. 11 000 water molecules. The TIP3P water model was used.[49] The system was neutralized by adding five chloride counterions.

Energy was minimized during 1000 steps using the steepest descent method for 100 steps and the conjugate gradient method

dx.doi.org/10.1021/jp304276v | J. Phys. Chem. B 2012, 116, 7827−7840

for 900 steps. Minimization was repeated three times, all atoms being allowed to move during the procedure, a nonbonding cutoff radius of 8.0 Å being used.

The system was heated from 0 to 300 K over 50 ps with a 0.2 fs time step under the *NVT* ensemble condition. For temperature regulation the Langevin thermostat was used with a collision rate of 2.0 ps^{-1}. Restraint force constants of 2.0 kcal mol^{-1} $Å^{-2}$ were used for all heavy atoms except the oxygen atoms of water molecules. To avoid instabilities in the simulation, NMR weight restraints were used to increase linearly the value of temperature from 0 to 300 K, thus ensuring that the system was heated in a controlled way.

Equilibration at 300 K was done in two steps under the *NPT* conditions: first, for 50 ps, with the restraint force constant of 2.0 kcal mol^{-1} $Å^{-2}$ for all heavy atoms except the oxygen atoms of water molecules; second, for 50 ps, with all atoms allowed to move. Finally, unrestrained MD was run over 0.5 ns at 1 atm and 300 K under the *NPT* conditions. The SHAKE algorithm was applied to constrain all covalent bonds involving hydrogen atoms. A time step of 2.0 fs and a nonbonding interaction cutoff radius of 8.0 Å were used at this stage of the procedure. Coordinates were saved every 1.0 ps during the entire process.

Nicotine Docking. The lowest energy structure obtained in the 0.5 ns unrestrained MD run was taken for the docking of nicotine. Ligand docking simulations were performed using ArgusLab 4.0.1 with the scoring method AScore. Water molecules and inorganic ions were removed before docking. The position of the 2-(3-pyridyl)furan ligand was used to define a binding pocket. The grid size was set to be 20 Å × 19 Å × 19 Å with a grid spacing of 0.4 Å. The lowest energy poses of the reactant were chosen for the further studies. The choice was based on the donor−acceptor distances for the effective hydrogen atom transfer. For neutral (2′*S*)-nicotine, two distances corresponding to H abstraction from the methyl carbon and from the carbon C5′ were taken into account. For protonated (2′*S*,1′*R*)-nicotine·H^+, only H abstraction from the methyl group was considered.

Three models were prepared initially: model A, the structure chosen for modeling H-abstraction from the C5′ position of neutral (2′*S*)-nicotine; model B, the structure chosen for modeling H-abstraction from the *N*-methyl position of neutral (2′*S*)-nicotine; model C, the structure chosen for modeling H-abstraction from the *N*-methyl position of protonated (2′*S*,1′*R*)-nicotine·H^+ (Chart 2).

Molecular Dynamics Preparation of Models for QM/MM Calculations. Molecular dynamics simulations were performed as described above for all three models. The production run simulations were performed during 2 ns. Minimum energy structures were taken for the next step. Noncrystallographic water molecules and inorganic ions were removed.

Further models used were model D, in which one molecule of crystallographic water was retained in the active site (Chart 2), and model E, in which the pyridine ring was flipped 180° around the C2−C3−C2′−N1′ dihedral angle with respect to its position in model B.

QM/MM Calculations. A sphere built from amino acids located around axial ligands and heme was defined with radii taken as shown in Table 1.

Within the selected radii, 77 amino acids (LEU62 ARG72 GLN75 ALA76 THR77 PHE78 ASP79 VAL81 PHE82 GLY86 VAL87 VAL88 PHE89 SER90 ALA95 ARG99 SER102 ILE103 LEU106 VAL111 ILE153 MET176 ILE179 PHE180 THR183 SER184 LEU212 LEU215 MET264 THR265 THR266 LEU267 ASN268 LEU269 PHE270 ILE271 GLY272 GLY273 THR274 GLU275 THR276 VAL277 THR279 THR280 GLN331 VAL336 ILE337 PRO338 MET339 SER340 LEU341 ALA342 ARG343 LEU366 VAL401 PRO402 PHE403 SER404 ILE405 ARG408 ASN409 CYQ410 PHE411 GLY412 GLU413 GLY414 LEU415 ALA416 ARG417 GLU419 LEU420 GLY450 PHE451 ALA452 THR453 ILE454) and 16 water molecules were included. During molecular dynamics simulation, one molecule of water drifted close to the oxygen of Cpd I. This molecule was kept only in one ONIOM[50] model (model D) aimed to describe methyl-H abstraction from (2′*S*)-nicotine assisted by one catalytic molecule of water. This molecule was removed from all other models before the ONIOM calculations. The cut protein chain was filled with C- and N-termini. The final structures contained 1633 and 1634 atoms for neutral and protonated nicotine, respectively. A total of 110 heavy atoms located on the surface of the sphere were kept frozen during the ONIOM simulations.

The QM part chosen for both models consisted of the truncated heme, −SMe (cysteine model) and nicotine, giving in total 69, 69, 70, 72, and 69 atoms for models A−E, respectively. Dangling bonds between both layers were saturated with hydrogen atoms. For the QM part, the B3LYP[51−55] method was applied in combination with the double-ζ quality LACVP basis set[56,57] for Fe and the 6-31G(d) basis set for the other atoms (later called B1) with mechanical embedding formalism. The real part of the model was treated at the MM level with the Amber force field[58] implemented in Gaussian09.[59] Nonstandard parameters compatible with the Amber force field for neutral and protonated nicotine and for Cpd I were the same as those used for the MD runs. Frequency calculations were performed for all complexes. No artificial imaginary frequencies for any of the complexes were obtained despite the freezing of the position of some atoms after the MD simulations. All transition states were characterized by only one imaginary frequency. The validity of transition states was confirmed by an intrinsic reaction coordinate (IRC)[60] scan in both directions. IRC scans in the forward direction for transition states of hydrogen atom transfer yielded radical intermediates (INT) having hydrogen of the hydroxyl group directed toward the hydrogen donor (C5′ for model A, and C_{Me} for models B−E, Chart 2). During optimization of INT to minimum, loose interaction between the hydrogen donor and transferred hydrogen was not preserved because of the reorientation phase[61] in which hydrogen rotates around the O−Fe axis together with the hydrogen donor: the later forming a C−O interaction. However, in the case of model A in the doublet spin state, the reorientation phase and a rebound step appear to be concerted: optimization to minimum results in hydrogen rotation followed by the spontaneous rebound step and formation of product. Single point energy calculations were carried out with a higher basis set: triple-ζ quality LACV3P+* on iron and the 6-31G(d) basis set on the other atoms (later called B2) with electronic embedding formalism.[62]

Because the active species of CYP2A6, Cpd I, involves two spin states (i.e., the high-spin quartet state and the low-spin doublet state), the ONIOM calculations were carried out on both the quartet (HS) and the doublet (LS) states to explore the possible reaction pathways (see Table SI2, Supporting Information, for the total charges and multiplicity). Relative energies were calculated at the ONIOM(B3LYP/B2:Amber) level with electronic embedding formalism and include ZPE correction.

Calculation of Isotope Effects. Optimized reactant and transition-state geometries and corresponding frequencies were

Chart 2. Models Employed for the Calculation of the Reaction Pathway for H-Abstraction from (2′S)-Nicotine (Models A, B, and D) and from (2′S,1′R)-Nicotine·H$^+$ (Model C)[a]

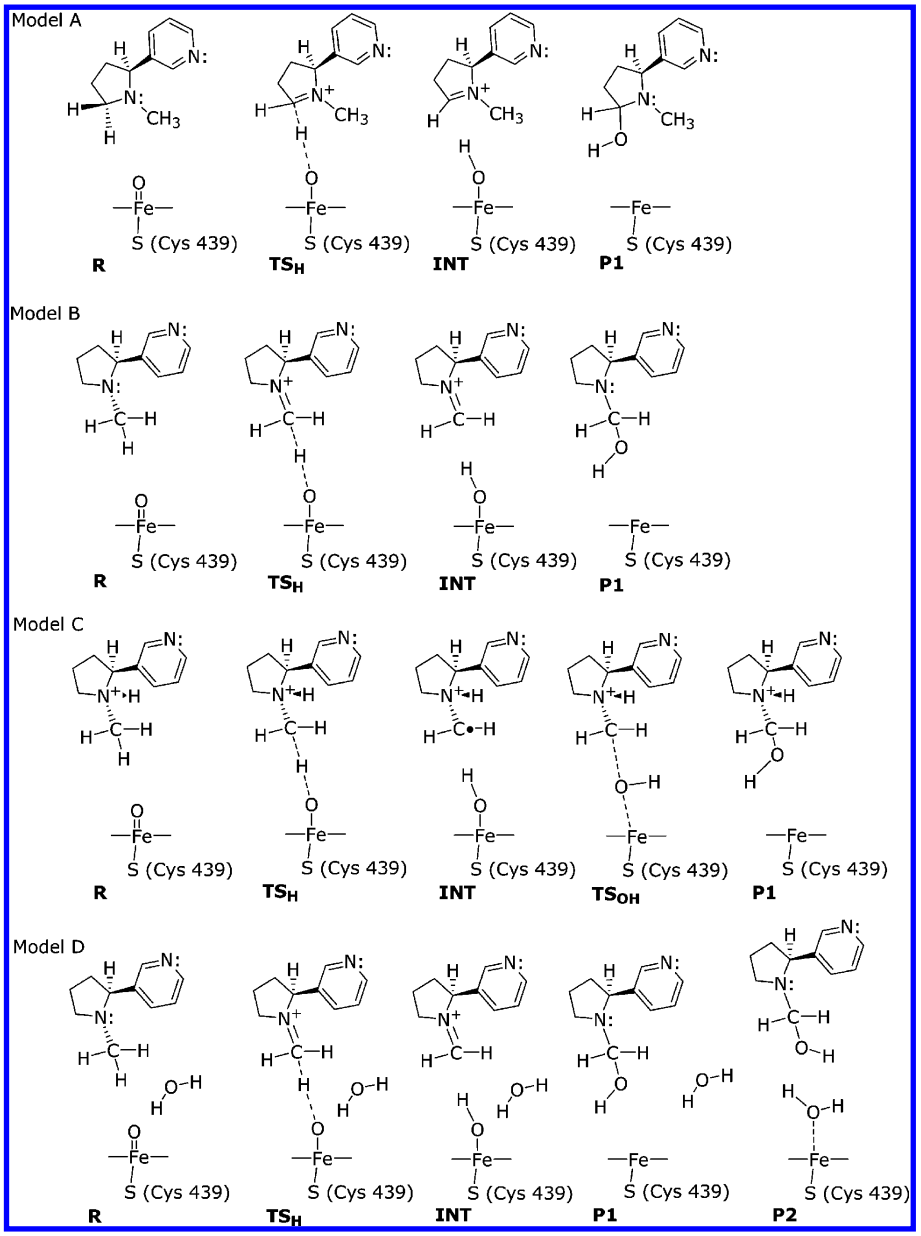

Table 1. Sphere Radii from Heme and Ligand Atoms that Delineate the Amino Acids included in the Active Site Pocket[a]

atom type	CBB	CBC	CGA	CGD	OQ	N1	N2	SG	O
residue	HEM	HEM	HEM	HEM	OFE	NIC	NIC	CYS	CYS
radius (Å)	6	6	6	6	10	10	10	10	10

[a]Heme (HEM) and cysteine (CYS) have PDB atom types, nicotine (NIC) has atom types assigned by Antechamber, and the oxygen of Cpd I (OFE) has the atom type assigned by Rydberg et al.[43]

used to calculate theoretical ^{2}H, ^{13}C, and ^{15}N KIEs using the ISOEFF07 program[63] at 300 K according to the Bigeleisen equation:[64]

$$\frac{k_L}{k_H} = \frac{\nu_L^{\neq}}{\nu_H^{\neq}} \times \prod_i^{3n-6} \frac{u_{i,H}^R \sinh(u_{i,L}^R/2)}{u_{i,L}^R \sinh(u_{i,L}^R/2)} \times \prod_i^{3n-7} \frac{\nu_{i,L}^{\neq} \sinh(u_{i,H}^{\neq}/2)}{\nu_{i,H}^{\neq} \sinh(u_{i,L}^{\neq}/2)}$$

where the subscripts L and H indicate light and heavy isotopes, respectively, n is the number of atoms, $u_i = h\nu_i/k_BT$, where h and k_B are Planck and Boltzmann constants, respectively, T is the absolute temperature, and ν_i is the frequency of the ith vibrational mode. The superscripts R and $\neq$ indicate reactant and transition state, respectively.

One-dimensional Wigner correction for tunneling was applied.[65]

Measurement of ^{2}H Kinetic Isotope Effects. Experimental apparent ^{2}H kinetic isotope effects were measured using liver microsomes isolated from phenobarbitone-treated rats. The incubation conditions were as follows: microsomes 0.5 mg/mL protein; nicotine 100 μM; NADPH regenerating system consisting

dx.doi.org/10.1021/jp304276v | J. Phys. Chem. B 2012, 116, 7827−7840

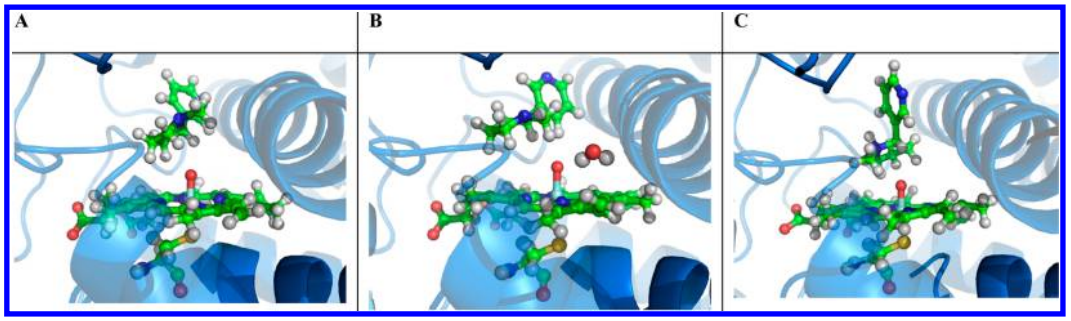

Figure 1. Snapshots of the active site of human CYP2A6 in complex with nicotine chosen from 2 ns MD to model (A) oxidation on the carbon C5′ of (2′*S*)-nicotine (model A), (B) N-demethylation reaction of (2′*S*)-nicotine (models B, D, and E), and (C) N-demethylation reaction of (2′*S*,1′*R*)-nicotine H^+ (model C). Nicotine and Cpd I are shown in ball-and-stick representation. Atoms: C (green), N (blue), O (red), Fe (cyan), S (yellow), H (white). Figures were prepared with PyMol 0.99rc6.69.

of glucose-6-phosphate 10 mM, $NADP^+$ 1 mM, glucose-6-phosphate dehydrogenase 5 U/mL; human cytosol 3 mg/mL protein (to provide aldehyde oxidase). Incubations were conducted at 37 °C for varying times between 30 and 90 min, with each time point in duplicate. Isotope effects were measured with either [4′,4′,5′,5′-$^2H_4$]nicotine or [methyl-$^2H_3$]nicotine at 1:1 with the undeuteriated species. After the appropriate time interval, incubation was stopped by adding the same volume of cold acetonitrile and centrifugation at 3000*g*. The ^2H:^1H isotope ratio in the residual substrate and in the product accumulated (as appropriate) was determined by LC−MS. The apparatus consisted of a Bruker Esquire ion trap connected to an Agilent LC1100 system working at room temperature with a 2.1 × 150 mm Dionex Acclaim Mixed mode HILIC-1 3 μm at a flow rate of 200 μL/min in an isocratic mode of 20% ammonium formate 100 mM pH 2.7 and 80% acetonitrile. The ion trap was set at 4500 V in positive mode with drying gas set at 40 psi and an auxiliary gas of 3 L/min, the cone temperature was set at 345 °C, and the trap opening was set at 4 *m*/*z*. Data acquisition was done either for 100 000 ions or 10 ms. Signal optimization was performed with 50/50 water/acetonitrile nicotine infusion. In all cases the degree of advancement of the reaction was low (<5%), so KIEs were only calculated from the isotope ratio of the product.

RESULTS AND DISCUSSION

Binding of (2′*S*)-Nicotine in CYP2A6 in Relation to C5′-H or Methyl-H Abstraction. No crystal structure of the human cytochrome P450 isoform 2A6 in complex with nicotine is available. Therefore, the X-ray structure PDB ID 2FDV, which contains the inhibitor *N*-methyl(5-(pyridin-3-yl)furan-2-yl)methanamine (D2G) in complex with CYP2A6 was chosen. This PDB entry also offers the highest resolution CYP2A6 X-ray structure available (1.65 Å). This PDB entry was suitable to transform the resting state of the cofactor to compound I, CYP450 O═Fe(IV) (Cpd I). (2′*S*)-nicotine was then docked into the active site. Prior to the QM/MM calculations, the complex was relaxed during 2 ns MD (Figure SI2, Supporting Information).

Model B (C_{Me}-H abstraction) remained stable during the 2 ns MD simulation (Figures SI2 B,D, Supporting Information), whereas in model A (C5′-H abstraction) a small rotation of the ligand during the first 300 ps of the production run caused shortening of the C5′−O(Cpd I) (later called D1) distance and elongation of the C(Me)−O(Cpd I) (later called D2) (Figures SI2 A,C, Supporting Information). Snapshots characterized by the lowest energies were chosen for the QM/MM calculations (Figure 1).

As can be seen in Figure 1, the orientations adopted by the neutral (2′*S*)-nicotine relative to Cpd I for the different H-abstraction reactions are similar, but not identical. The pyrrolidine of (2′*S*)-nicotine in model A is present in an envelope conformation with the nitrogen N1′ pointing out of the θ_2(C2′−C3′−C4′−C5′) (−6.22°) plane. This geometry is close to the ^1E conformer of pyrrolidine as defined by Martin et al.,[66] where the pyridine moiety is in the trans position relative to the methyl group. The position of the N1 pyridine nitrogen is defined by the dihedral angle χ(H2′−C2′−C3−C2) (8.58°), typical of a quasi-perpendicular arrangement of the two rings. (2′*S*)-Nicotine in model A adopts conformation ^1E. In model B, the pyrrolidine moiety is also in an envelope conformation, the C2′ carbon atom pointing down relative to the θ_3(C3′−C4′−C5′−N1′) (−0.89°) plane. The N1 pyridine nitrogen is trans to the methyl group, the two rings being quasi-perpendicular. It is worth noting that the N1 pyridine nitrogen is in the opposite direction to that in model A (χ = 168.73°). Let the conformation of (2′*S*)-nicotine in model B be assigned as E_2. The same geometry of nicotine is used in model D.

The structure chosen to model the C5′ oxidation reaction has D1 = 3.49 Å, D2 = 4.24 Å, O═Fe = 1.75 Å and Fe—S = 2.33 Å (Figure 1A), whereas that chosen to model the N-demethylation reaction has D1 = 4.33 Å, D2 = 3.34 Å, O═Fe = 1.73 Å and Fe—S = 2.31 Å (Figure 1B). Thus, the hydrogen atoms of the methyl group are initially placed closer to the O═Fe in model A than in model B. Conversely, the C5′ *trans*-H is closer to the O═Fe in model B. It should be noted that, in our model B the C5′ *cis*-H is too distant from the O═ Fe to interact, in contrast to the results obtained by Li et al.[34] for CYP2A6 but equivalent to the findings in CYP450 101.[36]

The difference in positioning is, in contrast, marked when protonated (2′*S*,1′*R*)-nicotine·H^+ is introduced into the active site (model C) (Figure 1C). Now the pyridine ring is seen to be pushed away from the heme, adopting a position virtually perpendicular to that in models A and B (χ(H2′−C2′−C3−C2) = 6.18°) but conserving its trans orientation with respect to the methyl group. Pyrrolidine preserves its envelope conformation with carbon C4′ pointing out of the plane of θ_0(C5′−N1′−C2′−C3′) (−5.94°). Let the conformation of (2′*S*,1′*R*)-nicotine H^+ be assigned as ^4E.[66]

A notable difference between models A and B is that the pyridine N1 adopts diametrically opposed positions: distal to the heme in model A and orientated toward the heme in model B. The importance of this parameter was investigated (see below) by manual rotation of the pyridine group through 180° around the C2−C3−C2′−N1′ dihedral angle (model E). Overall, the (2′*S*)-nicotine conserves the conformation E_2, with the pyrrolidine moiety close to and nearly parallel with the cytochrome, whereas the pyridine ring is twisted through 180°

dx.doi.org/10.1021/jp304276v | *J. Phys. Chem. B* 2012, 116, 7827−7840

around the inter-ring C−C bond between models A and B to obtain χ close to zero. This quasi-perpendicular position was found as the most stable conformation of nicotine in the isolated state;[67−69] however, there are no experimental data concerning the conformation of nicotine during its metabolism by the CYP450. This conformation is also comparable to that found by Li et al.[34] (Figure 1A) for 5′C *trans*-H abstraction.

Thus, it can be deduced that the primary factor contributing to the choice of H-abstraction is the positioning of the nicotine within the active site, and that this is perturbed by the presence of a charge on the pyrrolidine nitrogen. The active site of CYP 2A6 is relatively small and hydrophobic[70] and has only one polar amino acid, ASN297, of which the side chain can be used both as a hydrogen bond donor and as an acceptor. Flexible phenylalanine residues in the active site can contribute to the stabilization of the bound substrate by π-electron interactions between aromatic amino acid phenyl rings and unsaturated moieties (such as the pyridine ring of nicotine) of the bound substrate. These two types of interactions have been postulated to play a major role in the positioning of inhibitors close enough to the iron for efficient inhibition.[39] It has been shown experimentally that a number of other active site amino acid residues play a key steric role in modulating ligand affinity in CYP2A6.[71]

ONIOM Studies. Docking and subsequent MD simulations generated reliable structures of the human CYP2A6 in complex with (2′*S*)-nicotine. Exploiting these initial structures, the potential energy path for each of the oxidation reactions was obtained by the ONIOM hybrid method. From these, isotope effects associated with the two pathways of nicotine degradation have been calculated.

C5′-H Abstraction Studies—Model Validation. The models used and the results obtained were validated by comparison with the recently published work of Li et al.,[34] who used similar protocols for their QM/MM studies of the C5′ oxidation of (2′*S*)-nicotine, but with the addition that a whole protein model was used and all heme atoms were included in the QM region. In the first place, therefore, we have verified the geometries obtained for the abstraction of the C5′ *trans*-H from neutral (2′*S*)-nicotine (model A) by comparison with the models previously published.[34] The ONIOM QM/MM starting model system of the abstraction of the C5′ *trans*-H from neutral (2′*S*)-nicotine, based on model A, has been built from the docking structure with the lowest energy and with the shortest distance between the oxygen of Cpd I and the carbon C5′ and using the lowest energy structure taken from the MD simulation. Thus, the truncated model contained the same amino acids as models used for N-demethylation. The energy profiles obtained for the doublet (LS) and quartet (HS) spin states are illustrated in Figure 2A. The energy barriers obtained for the TS_H of 12.5 and 14.9 kcal/mol in the LS and HS states, respectively, are in fairly good agreement with those calculated by Li et al. (14.1 and 16.9 kcal/mol for LS and HS states, respectively).[34] These values represent the energy required for the effective transfer of the hydrogen atom from the carbon C5′ of (2′*S*)-nicotine to the O═Fe species of Cpd I. The reaction from reactant (R) to radical intermediate (INT) is thermo-neutral with energy of −1.0 kcal/mol for the quartet spin state, again in good agreement with Li (−2.0 and −0.1 kcal/mol for LS and HS states, respectively).[34]

The second part of the reaction on the C5′ carbon atom, which corresponds to the rebound of the hydroxyl group to C5′, is barrierless and very exothermic. Li et al. described a TS_{OH} corresponding to the rotation of the hydrogen of the hydroxyl group for both *trans*-H and *cis*-H abstraction, although in no case did this differ in energy from the INT state by more than 1 kcal/mol.[34] Obtaining the TS for this near-barrierless transfer proved not possible in the present study. However, as indicated by the reported values, it would not present any barrier to reaction kinetics and therefore is not important for an analysis of kinetic isotope effect parameters.

Overall, then, the structure obtained in the present study for the abstraction of the C5′ *trans*-H from neutral (2′*S*)-nicotine is in good agreement with that previously described.[34] The slight disparity observed can be explained by a number of factors: (i) the small differences in the geometries used, which derive from the higher resolution PDB file used here, (ii) different partial charges and force field parameters for Cpd I and reactants, (iii) minor differences in the docking of nicotine in the active site,[72] and (iv) the different calculation protocols employed.

C5′−H versus C_{Me}-H abstraction—Model A versus Model B. Thus, with model A validated by the above comparison, it is possible to compare directly the energy profile for nicotine C5′ *trans*-H abstraction (model A) with that for H-abstraction from the *N*-methyl group (model B). The barrier for the oxidation on the methyl group is 16.6 and 20.9 kcal/mol in the LS and HS states, respectively. This is the first report of these values determined by a QM/MM approach for neutral (2′*S*)-nicotine, now recognized as the probable molecular species for the reactions. Furthermore, they are significantly higher than for the abstraction of the C5′ *trans*-H by 4.1 and 6.0 kcal/mol, in the LS and HS states, respectively (Figure 2). Thus, the QM/MM results obtained for neutral and protonated nicotine indicate the same trends as those found in the small QM models.[32]

The second part of the reaction on the *N*-methyl group, consisting of the rebound of the hydroxyl group to C_{Me}, is barrierless and very exothermic. Overall, the rebound process is initiated by the elongation of the S−Fe bond leading to the elongation of the O−Fe and O−C_{Me} distances and to the lowering of the energy of the system. Subsequent small changes in the S−Fe distance and in the dihedral angle (C−CA−CB−S) of the cysteine ligated to iron precede rotation of the hydroxyl hydrogen by about 80°. The product molecule has an energy ca. 30 kcal/mol lower than the starting structure. As previously discussed, this can be assigned to electronic redistribution in the cytochrome ring, rather than to the reaction product.[73,74]

Protonation State of Nicotine for C_{Me}-H Abstraction—Model B versus Model C. Having energy differences of 4.1 kcal/mol (LS) and 6.0 kcal/mol (HS) between oxidation on the methyl group (C_{Me}) and on the carbon C5′ (Figure 2A,B), it is pertinent to ascertain the influence of the protonation state of nicotine on the choice of the oxidation center within the CYP2A6 active site. It was concluded that for QM small models the protonated state was favored both for C5′ *trans*-H and for *N*-methyl H abstraction.[32] Might, therefore, protonation of the pyrrolidine nitrogen direct reaction toward N-demethylation when the enzyme environment is taken into account? A barrier for this reaction was calculated for the oxidation on the carbon C_{Me} of the protonated (2′*S*,1′*R*)-nicotine·H^+. Two transition states were identified (Figure 2C). The first TS, corresponding to the hydrogen atom transfer from the methyl group of (2′*S*,1′*R*)-nicotine·H^+ to the oxo−iron species of Cpd I, has energy barrier values of 28.1 and 29.1 kcal/mol for the LS and HS states, respectively, and is the rate-limiting step for the reaction from R to product (P). These values are significantly higher than the corresponding barrier for neutral (2′*S*)-nicotine by 11.5 and 8.2 kcal/mol for the LS and HS states, respectively (Figure 2B,C).

dx.doi.org/10.1021/jp304276v | J. Phys. Chem. B 2012, 116, 7827−7840

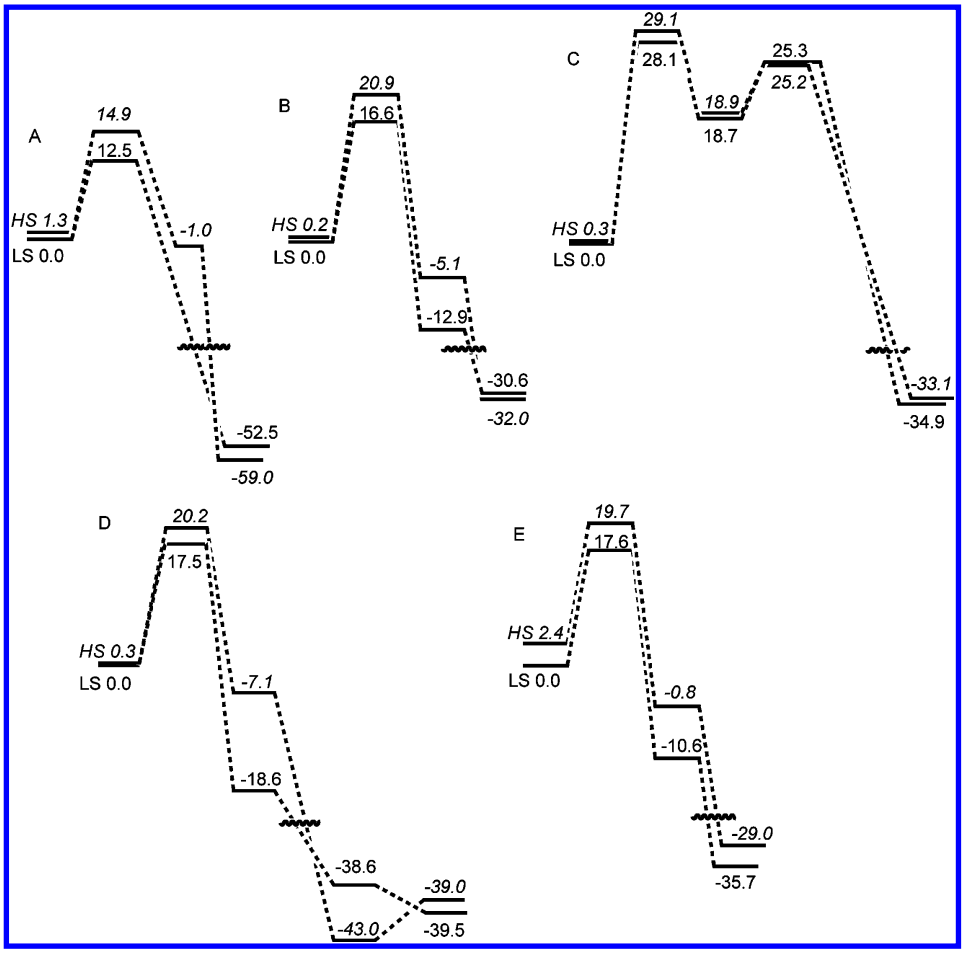

Figure 2. Energy profiles (kcal/mol) for the oxidation of nicotine by CYP2A6: (A) oxidation on the carbon C5′ of (2′*S*)-nicotine; (B) oxidation on the methyl group of (2′*S*)-nicotine; (C) oxidation on the methyl group of (2′*S*,1′*R*)-nicotine·H^+; (D) oxidation on the methyl group of (2′*S*)-nicotine in the presence of one molecule of water; (E) oxidation on the methyl group of (2′*S*)-nicotine with the pyridine moiety flipped by 180° around the N1′−C2′−C3−C2 angle. Relative energies were calculated at ONIOM(B3LYP/B2:Amber) level with electronic embedding formalism and include ZPE correction. As a reference, a doublet spin state (LS) of the complex of Cpd I with nicotine was used. LS, low-spin-state path; HS, high-spin-state path (in italics).

Additionally, conversion of (2′*S*,1′*R*)-nicotine·H^+ from the state R to the state INT is endothermic. As found for the QM model,[32] a second transition state corresponding to the rebound step of the hydroxyl radical is also obtained. This barrier is much lower: only 6.6 and 6.3 kcal/mol in the LS and HS states, respectively, is needed to activate this step. Overall, reaction from INT to P is very exothermic, as previously found.[73,74]

On the basis of this evidence, it is manifest that protonation of nicotine does not favor the abstraction of the methyl-H, because the barrier is much higher than for the neutral state. This is mainly due to the loss of the electron pair on the nitrogen N1′ (next to the hydrogen donor) as a result of protonation. It is apparent that this lone pair stabilizes the TS of the H-atom transfer from (2′*S*)-nicotine to Cpd I. With (2′*S*,1′*R*)-nicotine·H^+ this type of stabilization is impossible.

Role of a Molecule of Water during Catalysis—Model B versus Model D. It has been postulated that a molecule of water, which is hydrogen-bonded to the oxygen of the Cpd I, may play a catalytic role in P450 oxidation by acting to lower the energy barrier by ca. 2−4 kcal/mol in the QM/MM environment compared with the QM alone.[75] Therefore, the energy path was calculated with a molecule of water added to the ONIOM higher (QM) layer (Figure SI6, Supporting Information) to verify whether the presence of water so close to the reaction center might appreciably lower the energy barrier for N-demethylation, making this reaction pathway more competitive with oxidation on the carbon C5′. This molecule of water is kept in place during the MD production run by the hydrogen bonds formed with the oxygen atom of Cpd I, THR305, and the backbone carbonyl of GLY301 (Figure 1B).

Surprisingly, the presence of the water molecule did not influence significantly the energy barrier, the corresponding values being only +0.9 and −0.7 kcal/mol different in the LS and HS states, respectively, by comparison to the same model without water (Figure 2B,D). Furthermore, the water molecule is not found to take part in the stabilization of the TS (Figure 2D). However, reaction from R to INT is more exothermic, by 5.7 and 2.0 kcal/mol for the LS and HS states, respectively, and the radical intermediate in the LS is significantly more stabilized in the presence of water. Conversion of the radical intermediate to the product leads to two conformations of the product P inside the active site. In one, characterized by a better stabilization of the product in the HS state (by 4.4 kcal/mol compared with the LS state), nicotine-CH_2OH is coordinated with the iron of the heme by oxygen, whereas water is still hydrogen bonded with this oxygen. In the other, nicotine-CH_2OH is replaced by the water molecule coordinated with iron creating heme in the resting state, whereas product is still present in the active site. The doublet spin state is preferred over the quartet one by 2.7 kcal/mol for this stage of the process.

dx.doi.org/10.1021/jp304276v | *J. Phys. Chem. B* 2012, 116, 7827−7840

Table 2. Atom Pair Distances (Å) and a Donor−H−Acceptor Angle (deg) for the Transition-State Geometry during Oxidation of Nicotine, Calculated at the ONIOM(B3LYP/B1:Amber) Level of Theory with Mechanical Embedding[a]

model		atom pair distances (Å)						donor−acceptor angle (deg)
		N1′−C5′	N1′−C_{Me}	C−H	O−H	O−Fe	Fe−S	C−H−O
A	LS	1.412	1.45	1.286	1.305	1.711	2.478	169.2
	HS	1.41	1.45	1.339	1.259	1.72	2.392	161.8
B	LS	1.462	1.396	1.257	1.35	1.707	2.395	159.7
	HS	1.462	1.395	1.32	1.275	1.72	2.355	158.6
C	LS	1.518	1.472	1.774	1.011	1.783	2.423	156
	HS	1.518	1.473	1.736	1.018	1.777	2.44	158.1
D	LS	1.457	1.393	1.238	1.402	1.714	2.399	160.2
	HS	1.456	1.392	1.286	1.328	1.739	2.343	160.3
E	LS	1.471	1.396	1.289	1.298	1.713	2.412	157.5
	HS	1.471	1.397	1.33	1.261	1.72	2.36	157.5

[a]Note: distances for all structures are illustrated in Figures SI3−SI7 of the Supporting Information.

Table 3. Kinetic Isotope Effects Calculated for the Oxidation of Nicotine on the Carbon C5′ or on the Methyl Carbon (C_{Me}) for the Low-Spin (LS) and High-Spin (HS) States

	position for H abstraction									
	C5′ (model A) (2′S)-nicotine (E_2)[a]		C_{Me} (model B) (2′S)-nicotine (^1E)		C_{Me} (model C) (2′S,1′R)-nicotine·H^+ (E_1)		C_{Me} (model D) (2′S)-nicotine (E_S)·H_2O		C_{Me} (model E) (2′S)-nicotine (^1E)	
	^2TS_H (E_2)[b]	^4TS_H (E_2)	^2TS_H (E_S)	^4TS_H (^4E)	^2TS_H (E_1)	^4TS_H (E_1)	^2TS_H (E_S)	^4TS_H (E_S)	^2TS_H (^4E)	^4TS_H (^4E)
$^2H_1$[c,d]	8.38	9.92	6.00	8.27	2.72	3.24	4.77	8.05	7.34	8.67
$^2H_2$[d,e]	9.32	11.14	1.13	1.14	1.59	1.58	1.14	1.12	1.14	1.17
$^2H_3$[d,f]			6.88	9.69	4.42	5.21	5.46	9.21	8.58	10.40
$^{15}N1'$	0.9978	0.9979	1.0021	1.0018	1.0058	1.0052	1.0013	0.9999	1.0017	1.0030
$^{13}C2'$	1.0027	1.0027	1.0044	1.0041	1.0016	1.0016	1.0035	1.0033	1.0039	1.0041
$^{13}C5'$	1.0093	1.0104	1.0023	1.0025	1.0003	1.0004	1.0033	1.0028	1.0026	1.0028
$^{13}C_{Me}$	1.0000	0.9999	1.0078	1.0111	1.0486	1.0448	1.0062	1.0101	1.0095	1.0112

[a]Pyrrolidine ring configurations in the reactant states are indicated in parentheses, according to ref 66. [b]Pyrrolidine ring configurations in the TS_H are indicated in parentheses, according to ref 66. [c]^2H Substitution on the atom that is transferred. [d]Includes Wigner correction for tunneling.[65] [e]In model A, ^2H substitution on both atoms. In models B−E, ^2H substitution on the atoms that are not transferred. [f]^2H Substitution on all atoms.

Isotope Effects. *Geometries of Models for C5′-H or C_{Me}-H Abstraction and Kinetic Isotope Effects.* On the basis of these structures, the architectures of the structures for the abstraction of H from either the C5′ or the *N*-methyl positions and the associated isotope effects can be compared among the different models A−E. These are summarized in Tables 2 and 3, respectively, and given in full in the Supporting Information (Tables SI3−SI7).

Comparison of the Geometries and Kinetic Isotope Effects for C5′-H or C_{Me}-H Abstraction—Effect of H-Atom Position in Relation to Cpd I (Model A versus Model B). The architecture of the structures for the abstraction of H from the C5′ or the C_{Me} from (2′*S*)-nicotine are illustrated in Figure 3, and the parameters are summarized in Table 2. On the basis of these parameters, kinetic isotope effects were calculated (Table 3 and Tables SI3 and SI4, Supporting Information).

As can be seen from the C−H−O distances in the TS_H structures for models A and B, the TS_H for C5′ H abstraction is more symmetrical for both LS and HS states than that for C_{Me}-H abstraction, which is earlier (Table 2). This is reflected in the higher calculated $^2H_3$ KIE values for C5′-H abstraction. A number of other differences are apparent. Thus, the ^{13}C KIE for the C5′ position is, as might be anticipated for a primary effect, higher for abstraction of the C5′-H than for C_{Me}-H abstraction. Nevertheless, a small normal effect is seen for the C_{Me}-H abstraction, indicating that considerable electron dispersion occurs in both reaction pathways. This proposition is supported by the secondary ^{13}C KIEs also seen at the C2′ position for both reactions. Interestingly, the primary ^{13}C KIEs for the carbon at the position of bond breakage are similar for both reactions (1.0078 and 1.0093, for the C_{Me} and C5′, respectively). These values are well below the Streitwieser semiclassical limit (1.0210) for C−H bond breaking, suggesting that in both cases the carbon radical is partially stabilized in the TS. This stabilization apparently occurs in the same manner in both reactions: the sharing of electrons between nitrogen and carbon leads to stiffer connections between atoms, leading to a double bond character connection in the INT models (Figures SI3 and SI4, Supporting Information).

A notable distinguishing feature is the secondary ^{15}N KIE values, which are inverse for oxidation on C5′ (0.9978) and normal for oxidation on C_{Me} (1.0021). This inversion can be explained by a TS geometry wherein nitrogen is bound more or less stiffly than in the reactants. However, the evolutions in the geometries around N1′ from reactants to transition states are similar (Figures SI3− SI7, Supporting Information) but not identical for both reactions because of the location of the reaction center. For the reaction path leading to nornicotine, the reaction center is localized on the relatively mobile methyl group connected to N1′, whereas for the reaction toward cotinine, oxidized carbon C5′ belongs to the pyrrolidine ring, a more rigid environment. The distances N−C and C−H in the TS for abstraction from C_{Me}-H are only 0.02 Å shorter than those for abstraction from C5′-H, and the H---O distance is only 0.04 Å longer (Figures SI3 and SI4, Supporting Information). However, there is a substantial difference in the pseudorotation of the pyrrolidine ring in both species (Table 3). In model A, its

dx.doi.org/10.1021/jp304276v | J. Phys. Chem. B 2012, 116, 7827−7840

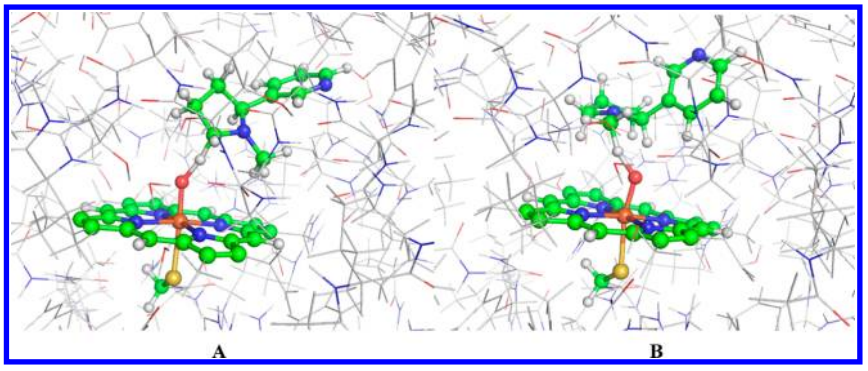

Figure 3. TS_H structures for the oxidation of (2′*S*)-nicotine to (A) 5′-hydroxynicotine (pathway to cotinine) and (B) *N*-hydroxymethylnornicotine (pathway to nornicotine) in the LS state.

reactant conformation (E_2) is conserved in the TS_H, whereas in model B, the pyrrolidine ring pseudorotates from (^1E) to (E_S) and (^4E), in the LS and HS states, respectively. The small inverse ^{15}N KIE of model A can result from the stiffer binding of nitrogen in the transition state, in which an iminium ion character develops, and can be stabilized by the inductive effect from C2′. The temperature independent factor (TIF), which is the ratio of the imaginary frequencies for the light to heavy reactants associated with the reaction coordinate motion, do not contribute to the ^{15}N KIE in either the LS or HS state (Table SI3, Supporting Information). It is, then, the temperature dependent factor (TDF) that dictates the value of the isotope effect, and for the tighter bonding in the TS than in reactants, the TDF becomes inverse. In the case of model B, steric isotope effects must be taken into account as the pyrrolidine ring pseudorotates. The $^{15}N1'$, $^{13}C2'$, and $^{13}C5'$ equilibrium isotope effects (EIEs) for pseudorotation of the pyrrolidine ring of (2′*S*)-nicotine between conformations ^1E and E_1 (Figure 4) were

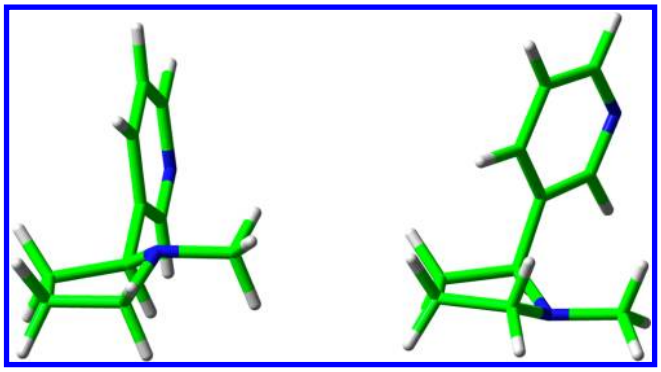

Figure 4. Equilibrium between two extreme envelope conformations of (2′*S*)-nicotine: ^1E (left) and E_1 (right) calculated in the gas phase at the B3LYP/6-311+G(d,p) level.

calculated in the gas phase (Table 4) to verify the magnitude of the isotope effect during pseudorotation between the two extreme conformations. Small normal effects of 0.2% were found for $^{15}N1'$ and $^{13}C2'$ and of 0.1% in $^{13}C5'$. Clearly, the secondary ^{15}N isotope effect is affected by the pseudorotation of the pyrrolidine moiety. In model D (Table 3), characterized by the presence of the water molecule, in which pseudorotation does not occur, effects on nitrogen N1′ are negligible (1.0013 and 0.9999 in the LS and HS, respectively): the ^{15}N KIE for the N-demethylation of (2′*S*)-nicotine by the CYP2A6 is then close to unity.

Table 4. Relative Energy (Δ*E*, kcal/mol with ZPE Correction) and Equilibrium Isotope Effects (EIE) Calculated for the Pseudorotation of the Pyrrolidine Ring of (2′*S*)-Nicotine between the Two Extreme Conformations ^1E and E_1[a]

Δ*E* (kcal/mol)	$^{15}N1'$ EIE	$^{13}C2'$ EIE	$^{13}C5'$ EIE
4.2	1.0021	1.0023	1.0014

[a]Values are calculated in the gas phase at the B3LYP/6-311+G(d,p) level.

Comparison of the Geometries and Kinetic Isotope Effects for C_{Me}-H Abstraction—Effect of the Presence of Water in the Active Site (Model B versus Model D). The architectures of the structures of the LS and HS states for C_{Me}-H abstraction in the presence of a molecule of water (model D) are illustrated in Figure 5, and the KIEs are presented in Table 3.

Water is involved in a hydrogen bond with the oxygen of Cpd I. This distance changes with the progress of the reaction. In the reactant state this hydrogen bond has distances of 1.835 and 1.833 Å in the LS and HS states, respectively, and becomes longer in the transition state (1.911 and 1.906 Å in the LS and HS states, respectively). The shortest values are observed for the radical intermediate (1.667 and 1.658 Å in the LS and HS states, respectively), which appears significantly stabilized in the presence of water. Two product states were observed. In the first, a strong hydrogen bond is retained between water and the oxygen of the −OH moiety and the oxygen of water approaches iron, such that it is closer than the −OH group of the product. In the second, product is separated from iron by water, which is coordinated to iron by oxygen with distances of 2.132 and 2.491 Å for the LS and HS states, respectively.

The TS_H is earlier in the presence of the one molecule of water in close proximity to the reaction center. Thus, ^2H KIEs are slightly smaller in model D than in model B where water was removed after MD simulation. Stabilization of the TS_H occurs in a similar way as in model B: better stabilization in the doublet spin state relative to the quartet was observed. A very small normal secondary ^{15}N KIE is seen in the LS state but none is observed in the HS state. Normal ^{13}C KIEs were also calculated for the C2′ and C5′, and values are similar to those of model B. No pseudorotation of the pyrrolidine ring was observed in the presence of water. The value of ^{15}N KIE is not affected by the conformational changes. The pyrrolidine nitrogen N1′ develops an iminium ion character in the TS as a result of losing an electron lone pair in the stabilization of the C_{Me} radical, without loss of its pyramidal geometry. N1′ is more tightly bound in the HS than in the LS state and the hydrogen atom transfer is more advanced in the former (Table 2).

dx.doi.org/10.1021/jp304276v | *J. Phys. Chem. B* 2012, 116, 7827−7840

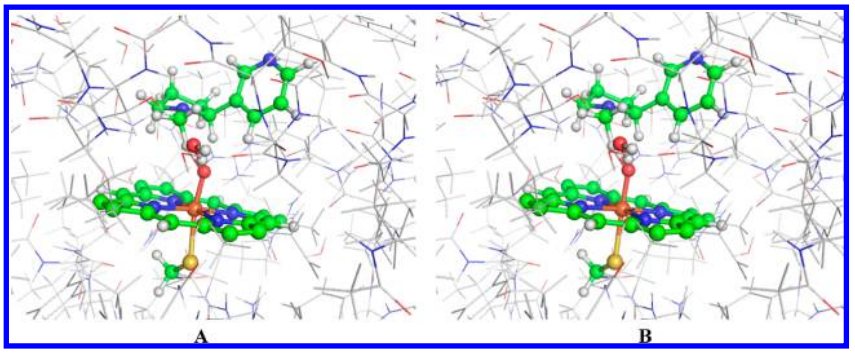

Figure 5. TS_H structures for the conversion of (2′*S*)-nicotine to *N*-hydroxymethylnornicotine in the presence of water: (A) LS state; (B) HS state.

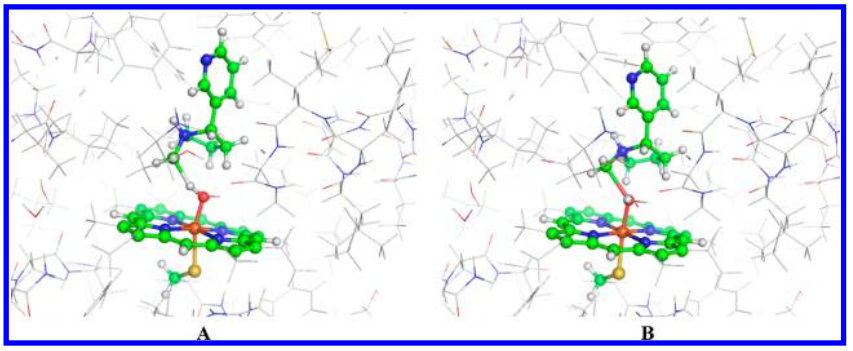

Figure 6. TS structures for the conversion of (2′*S*,1′*R*)-nicotine·H^+ to *N*-hydroxymethylnornicotine H^+ in the LS state: (A) TS_H; (B) TS_{OH}.

Comparison of the Geometries and Kinetic Isotope Effects for C_{Me}-H Abstraction—Effect of Protonation on the Pyrrolidine Nitrogen on C_{Me}-H Abstraction (Model B versus Model C). The architecture of the structures for the C_{Me}-H abstraction from (2′*S*,1′*R*)-nicotine·H^+ are illustrated in Figure 6, and the KIEs are presented in Table 3.

Oxidation of (2′*S*,1′*R*)-nicotine·H^+ to *N*-hydroxymethylnornicotine is characterized by two transition states. The first (TS_H) corresponds to the hydrogen atom transfer from the methyl carbon to the oxygen of Cpd I, and the second (TS_{OH}) to the −OH rebound from Fe back to the C_{Me}. The TS_H occurs later than in the case of (2′*S*)-nicotine (model B) (Table 2), a behavior reflected in smaller values of the ^2H KIEs found for both spin states. However, there is a significant normal primary ^{13}C isotope effect on the C_{Me} (1.0486 and 1.0448 for the LS and HS states, respectively) and a small normal secondary ^{15}N KIE (1.0058 and 1.0052 for the LS and HS states, respectively), showing significant diminution of the carbon radical stabilization in the protonated state. The TDF makes a higher contribution to the normal primary $^{13}C_{Me}$ KIE than does the TIF (Table SI5) and dictates the magnitude of this effect. As C_{Me} is more loosely bound in the TS_H than in reactants, TDF becomes normal.

It might be considered that, in a situation in which nicotine is protonated on the nitrogen of the pyrrolidine moiety and at least one molecule of water is in close proximity to the (2′*S*,1′*R*)-nicotine·H^+ bound inside the active site of P450, fast deprotonation could complicate any measured isotope effects. Reactant in the LS state from model B and the TS_H in the LS state of the model C were used to calculate ^{15}N and ^2H isotope effects. Calculated KIEs at N1′ show a significant inverse secondary ^{15}N KIE (0.9424), and a normal primary $^2H_3$ KIE (7.92 without Wigner tunneling correction). Thus, this hypothesis can be rejected on the basis of the experimental ^{15}N KIE for N1′ measured at natural abundance ^{15}N for the N-demethylation of *S*-nicotine and (*R*,*S*)-*N*-methyl-2-phenylpyrrolidine by *Nicotiana*.[31] In plants, the degradation of nicotine is known to be strongly selective for N-demethylation; hence the ^{15}N KIE can be used as a reference values for N-demethylation catalyzed by the CYP family. The ^{15}N KIEs obtained are small and normal: 1.0028 and 1.0032 for the N-demethylation of *S*-nicotine or (*R*,*S*)-*N*-methyl-2-phenylpyrrolidine, respectively.[31] These values are in good agreement with the theoretically predicted values for model B (1.0021 in the LS state), but not with those for model A. Thus, experimentally measured ^{15}N KIEs can be proposed as a sensitive probe of the oxidation center to differentiate between N-demethylation and oxidation on C5′.

Comparison of the Geometries and Kinetic Isotope Effects for C_{Me}-H Abstraction from (2′S)-Nicotine—Effect of Configuration of the Pyridine Ring (Model B versus Model E). Following the previous observation that the conformation of (2′*S*)-nicotine can be stabilized by hydrogen bonding of the pyridine nitrogen with the side chain of ASN297,[34] the influence of this alternative conformation was investigated. The architecture of the structure for H-abstraction from the C_{Me} of (2′*S*)-nicotine in conformation ^4E is illustrated in Figure 7, and the KIEs are presented in Table 3. No significant differences were observed between models B and E for the first step of hydrogen atom transfer (Table 2). The TS_H is slightly more central than in model B, but this has a minor impact on the theoretical KIE values (Table 3). Thus, conclusions concerning the mechanism of stabilization of the TS remain the same. Flipping of the pyridine moiety by 180° around the inter-ring bond to create a hydrogen bond with ASN297 does lower the energy barrier by ca. 1 kcal/mol, a barely significant effect. Hence, although ASN297 may play a role in the binding of nicotine, this does not appear essential for catalysis, and does not influence the choice of position for H-abstraction.

Comparison of the Apparent Experimental and Theoretical ^2H Kinetic Isotope Effects for C_{Me}-H or C5′-H Abstraction from (2′S)-Nicotine (Model A versus Model B). Apparent experimental competitive ^2H KIE were measured for the

dx.doi.org/10.1021/jp304276v | *J. Phys. Chem. B* 2012, 116, 7827−7840

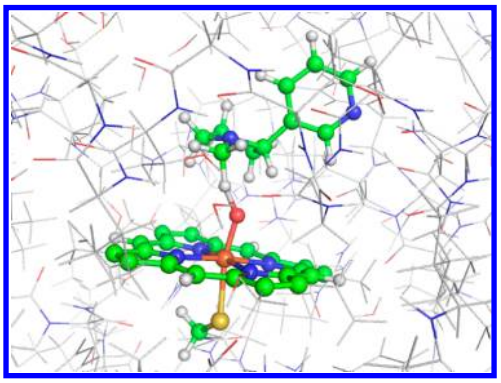

Figure 7. TS_H structure for the conversion of (2′*S*)-nicotine to *N*-hydroxymethylnornicotine (model E) in the LS state.

abstraction of H from the C_{Me} or the C5′ positions of (2′*S*)-nicotine (Table 5). In all cases, the degree of advancement of the reaction was low (<5%), so that isotope ratio changes could only be determined for the product.

Table 5. Apparent Experimental Competitive ^2H Kinetic Isotope Effects for C_{Me}-H or C5′-H Abstraction from (2′*S*)-nicotine

		product			
		cotinine		nornicotine	
substrate	incubation conditions	^2H KIE	SD	^2H KIE	SD
(2′*S*)-[4′,4′,5′,5′-$^2H_4$] nicotine (50% ^2H)	substrate			0.92	0.09
	substrate + cytosol	2.60	0.51	0.92	0.18
(2′*S*)-[methyl-$^2H_3$] nicotine (50% ^2H)	substrate			*a*	
	substrate + cytosol	2.28	0.46	*a*	

[a]Unable to measure the ^2H:^1H ratio in the product.

With (2′*S*)-[4′,4′,5′,5′-$^2H_4$]nicotine as substrate, nornicotine accumulation could be measured when no aldehyde oxidase was present (no cytosol added) and when cytosol was present (Table 5). In both cases, no significant isotope effect was observed, indicating that no secondary isotope effect at the 5′5′ positions was seen for the abstraction of an H atom from the C_{Me}. With (2′*S*)-[methyl-$^2H_3$]nicotine, the ^2H KIE for nornicotine production cannot be measured on the product and the reaction was insufficiently advanced to measure this on the substrate. In contrast, with both substrates, a significant ^2H KIE was determined for the formation of cotinine (Table 5). This appeared slightly higher when (2′*S*)-[4′,4′,5′,5′-$^2H_4$]nicotine was the substrate, but there was also a clear ^2H KIE with (2′*S*)-[methyl-$^2H_3$]nicotine. This would indicate that the presence of a ^2H in either the C5′ or the C_{Me} positions has a significant effect on the reaction kinetics. The values around 2.2−2.6 are considerably lower than those predicted by the theoretical calculations (9.3 and 6.9 for C5′ or the C_{Me} positions in the LS state of Cpd I). The fact that similar values are found for cotinine formation from both substrates, however, may indicate that the measured value is not just that for H-abstraction but, rather, is a combined value for ^2H influence on electronic redistribution between iminium states of the pyrrolidine ring (see above), secondary ^2H KIEs, and, in the case of (2′*S*)-[4′,4′,5′,5′-$^2H_4$]nicotine, a possible ^2H KIE for removal of the second H from the C5′ position by aldehyde oxidase. Thus, direct comparison between such apparent experimental ^2H KIE values and those predicted for the TS_H of models A and B must be treated with caution.

CONCLUSIONS

The overall conclusion of the present work, then, is that it is primordially the energy cost of H-abstraction that determines the relative selectivity between C_{Me}-H and C5′-H abstraction by Cpd I in the active site of CYP2A6. N-Demethylation leading to *N*-hydroxymethylnornicotine requires ca. 6.5 kcal/mol more energy to transfer a hydrogen atom than is required for oxidation on the carbon C5′. It remains an open question what are the exact parameters determining the relative energy barriers. Clearly, protonation of the N1′ pyrrolidine nitrogen is detrimental to C_{Me}-H abstraction, leading to an enhanced barrier of ca. 10 kcal/mol. This can be attributed to the loss of the lone electron pair on N′1 that can no longer participate in stabilizing the TS. Furthermore, a molecule of water in the active site of CYP2A6 does not aid in the stabilization of the TS_H for C_{Me}-H abstraction, nor does it influence the corresponding energy barrier. Similarly, H-bonding of the pyridine nitrogen to ASN297 does not have any effect on the energy barrier for H-abstraction from C_{Me}.

Examining the architecture of the active site does give some indication that C5′ is favored, as in this reaction a shorter donor/acceptor distance is found. However, no substantial protein conformational change associated with either reaction (post-substrate docking) that might otherwise aid in lowering the energy barrier is evidenced through the computational studies. A simulation of the positioning of the pertinent residues, the substrate and the cytochrome in the active site during the reaction for the different models indicated only minor displacements of some residues

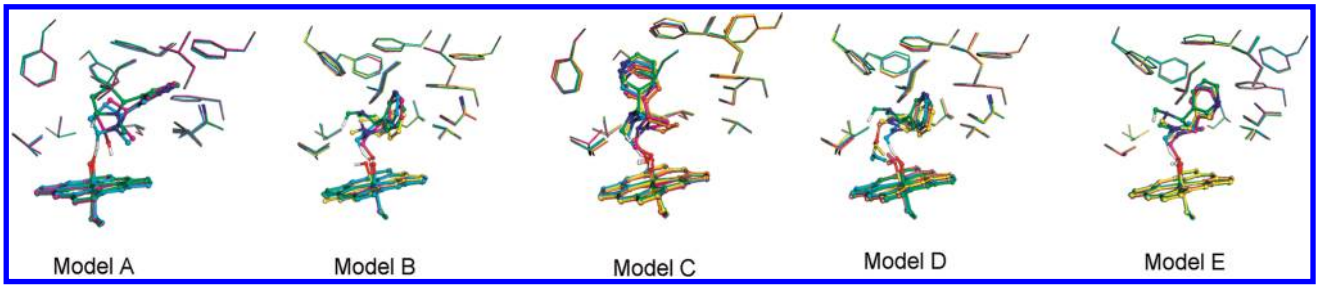

Figure 8. Active site architecture for the conversion of (2′*S*)-nicotine to *N*-hydroxymethylnornicotine (models B−E) or to 5′-hydroxynicotine (model A), all models shown in the LS state. Color coding: oxygen of Cpd I, red; nitrogen of nicotine and ASN297, blue; transferred hydrogen, gray. Other atoms are green for reactant, cyan for TS_H, yellow for INT, orange for TS_{OH} (only for model C), magenta for product, and pink for the second product (only for model D).

dx.doi.org/10.1021/jp304276v | *J. Phys. Chem. B* 2012, 116, 7827−7840

(Figure 8). Only in model C, in which N1′ is protonated does the nicotine adopt a significantly different orientation: this is reflected in both the unfavorable energetics and in the small ^{2}H KIE (Table 3).

In this study, we show that truncated ONIOM models are a good compromise between computational costs and reliable identification of the rate limiting step for the oxidation reactions catalyzed by the cytochrome P450 enzymes in the Cpd I form. This can be concluded from the good agreement obtained between our model A and the protocol previously carried out for the C5′-H abstraction.[34] However, we have taken the analysis further than previously, in comparing different reaction conditions and exploiting KIEs to probe the reaction mechanism. Two key features are apparent. First, the ^{13}C KIEs for H-abstraction from either C position indicate considerable electronic redistribution within the pyrrolidine ring to be taking place in both mechanisms, as evidenced by the significant normal ^{13}C KIEs at C2′ and C5′ (Table 3). However, a marked difference is that in model A (C5′-H abstraction) no KIE is seen at the C_{Me}, whereas in model B (C_{Me}-H abstraction) a significant ^{13}C KIE occurs at the C_{Me}. Differences in the electronic distribution in the pyrrolidine ring are also highlighted by the ^{15}N KIEs. Critically, the C_{Me}-H abstraction is associated with a negligibly-small normal value, whereas in C5′-H abstraction the ^{15}N KIE is small inverse. This is compatible with an iminium ion $^{+}$N1′=C character of the TS_H and preservation of the pyramidal geometry around the N1′ nitrogen caused by the steric constraints of the pyrrolidine ring for the oxidation of (2′*S*)-nicotine with tighter binding in C5′-H abstraction than in the N-demethylation reaction pathway (Table 2). Hence, it is demonstrated that a careful examination of the KIE values can lead to greater insights into the reaction mechanism than can be obtained by only considering the energy barriers.

■ ASSOCIATED CONTENT

Ⓢ Supporting Information

Modification to the CYP isoform 2A6 in complex with inhibitor. Molecular dynamics simulations. Atom pair distances (Å) and imaginary frequencies (cm^{-1}) calculated for the key points during oxidation on the carbon C5′ of (2′*S*)-nicotine. List of amino acids creating the CYP2A6 active site. Table of total charge and multiplicity assigned to the ONIOM layers for all studied models. Table of kinetic isotope effects and imaginary frequencies. This material is available free of charge via the Internet at http://pubs.acs.org.

■ AUTHOR INFORMATION

Corresponding Author

*E-mail: Richard.Robins@univ-nantes.fr.

Notes

The authors declare no competing financial interest.

■ ACKNOWLEDGMENTS

This research was supported by a Marie Curie Intra-European Fellowship (No. PIEF-GA-2008-219821) within the 7th European community Framework Program to R.A.K. and by an ANR grant to R.J.R. and M.D. (No. ANR-08-PCVI-0017). We are most grateful to the following for computational facilities and grants of computational times: R.A.K., CCIPL (Centre de Calcul Intensif des Pays de la Loire); P.P., ACK CYFRONET AGH (Krakow, Poland). This work was granted access to the HPC resources of [CCRT/CINES/IDRIS] under the allocation c2011085117 made by GENCI (Grand Equipement National de Calcul Intensif).

■ REFERENCES

(1) Ortiz de Montellano, P. R.; de Voss, J. J. In *Cytochrome P450, Structure, Mechanism and Biochemistry*; Ortiz de Montellano, P. R., Ed.; Kluwer Academic/Plenum Publishers: New York, 2005; pp 183−245.
(2) Shaik, S.; Cohen, S.; Wang, Y.; Chen, H.; Kumar, D.; Thiel, W. *Chem. Rev.* **2010**, *110*, 949−1017.
(3) Lewis, D.; Ito, Y. *Xenobiotica* **2009**, *39*, 625−635.
(4) Pochapsky, T.; Kazanis, S.; Dang, M. *Antioxid. Redox Signaling* **2010**, *13*, 1273−1296.
(5) WHO. *WHO Report on the global tobacco epidemic, 2011: warning about the dangers of tobacco*; World Health Organisation: Geneva, 2011.
(6) Rendic, S. *Drug Metab. Rev.* **2002**, 83−448.
(7) Nakajima, M.; Yamamoto, T.; Nunoya, K.; Yokoi, T.; Nagashima, K.; Inoue, K.; Funae, Y.; Shimada, N.; Kamataki, T.; Kuroiwa, Y. *Drug Metab. Dispos.* **1996**, *24*, 212−1217.
(8) Yamanaka, H.; Nakajima, M.; Fukami, T.; Sakai, H.; Nakamura, A.; Katoh, M.; Takamiya, M.; Aoki, Y.; Yokoi, T. *Drug Metab. Dispos.* **2005**, *33*, 1811−1818.
(9) Murphy, S. E.; Raulinaitis, V.; Brown, K. M. *Drug Metab. Dispos.* **2005**, *33*, 1166−1173.
(10) Kyerematen, G.; Morgan, M.; Chattopadhyay, B.; de Bethizy, J.; Vesell, E. *Clin. Pharmacol. Ther.* **1990**, *48*, 641−651.
(11) Yamanaka, H.; Nakajima, M.; Nishimura, K.; Yoshida, R.; Fukami, T.; Katoh, M.; Yokoi, T. *Eur. J. Pharm. Sci.* **2004**, *22*, 419−425.
(12) Di, Y.; Chow, V.; Yang, L.; Zhou, S. *Curr. Drug Metab.* **2009**, *10*, 754−780.
(13) Guengerich, F. In *Cytochrome P450, Structure, Mechanism and Biochemistry*; Ortiz de Montellano, P. R., Ed.; Kluwer Academic/Plenum Publishers: New York, 2005; pp 377−530.
(14) Smith, B.; Sanders, J.; Porubsky, P.; Lushington, G.; Stout, C.; Scott, E. *J. Biol. Chem.* **2007**, *282*, 17306−17313.
(15) Ding, X.; Kaminsky, L. *Annu. Rev. Pharmacol. Toxicol.* **2003**, *43*, 149−173.
(16) Bao, Z.; He, X.-Y.; Ding, X.; Prabhu, S.; Hong, J.-Y. *Drug Metab. Dispos.* **2005**, *33*, 258−261.
(17) Nordberg, A.; Hartvig, P.; Lundqvist, H.; Antoni, G.; Ulin, J.; Langstrom, B. *J. Neural. Transm. [P-D Sect]* **1989**, *1*, 195−205.
(18) Plowchalk, D.; Andersen, M.; de Bethizy, J. *Toxicol. Appl. Pharmacol.* **1992**, *116*, 177−188.
(19) Nyback, H.; Halldin, C.; Ahlin, A.; Curvall, M.; Eriksson, L. *Psychopharmacology* **1994**, *115*, 31−36.
(20) Crooks, P. A.; Li, M.; Dwoskin, L. P. *Drug Metab. Dispos.* **1997**, *25*, 47−54.
(21) Ghosheh, O.; Dwoskin, L.; Li, W.; Crooks, P. *Drug Metab. Dispos.* **1999**, *27*, 1448−1455.
(22) Siminszky, B.; Gavilano, L.; Bowen, S.; Dewey, R. *Proc. Natl. Acad. Sci., U. S. A.* **2005**, *102*, 14919−14924.
(23) Jones, J.; Trager, W.; Carlson, T. *J. Am. Chem. Soc.* **1993**, *115*, 381−387.
(24) Bernhardt, R. *J. Biotechnol.* **2006**, *124*, 128−145.
(25) Cojocaru, V.; Winn, P. J.; Wade, R. C. *Biochim. Biophys. Acta* **2007**, *1770*, 390−401.
(26) Gavilano, L. B.; Coleman, N. P.; Bowen, S. W.; Siminszky, B. *J. Biol. Chem.* **2007**, *282*, 249−256.
(27) Wang, S.; Yang, S.; An, B.; Wang, S.; Yin, Y.; Lu, Y.; Xu, Y.; Hao, D. *PloS One* **2011**, *6*, e23342.
(28) Karki, S. B.; Dinnocenzo, J. P. *Xenobiotica* **1995**, *25*, 711−724.
(29) Guengerich, F. P.; Yun, C.-H.; Macdonald, T. L. *J. Biol. Chem.* **1996**, *271*, 27321−27329.
(30) Dowers, T. S.; Rock, D. A.; Rock, D. A.; Perkins, B. N. S.; Jones, J. P. *J. Am. Chem. Soc.* **2004**, *126*, 8868−8869.
(31) Molinié, R.; Kwiecień, R. A.; Paneth, P.; Hatton, W.; Lebreton, J.; Robins, R. J. *Arch. Biochem. Biophys.* **2007**, *458*, 175−183.
(32) Li, D.; Wang, Y.; Han, K.; Zhan, C.-G. *J. Phys. Chem. B* **2010**, *114*, 9023−9030.
(33) Wang, Y.; Kumar, D.; Yang, C.; Han, K.; Shaik, S. *J. Phys. Chem. B* **2007**, *111*, 7700−7710.

(34) Li, D.; Huang, X.; Han, K.; Zhan, C.-G. *J. Am. Chem. Soc.* **2011**, *133*, 7416−7427.
(35) Carlson, T.; Jones, J.; Peterson, L. A.; Castagnoli, N. J.; Iyer, K.; Trager, W. *Drug Metab. Dispos.* **1995**, *23*, 749−756.
(36) Peterson, L. A.; Castagnoli, N. J. *J. Med. Chem.* **1988**, *31*, 637−640.
(37) Senn, H. M.; Thiel, W. *Angew. Chem., Int. Ed.* **2009**, *48*, 1198−1229.
(38) Usharani, D.; Zazza, C.; Lai, W.; Chourasia, M.; Waskell, L.; Shaik, S. *J. Am. Chem. Soc.* **2012**, *134*, 4053−4056.
(39) Yano, J. K.; Denton, T. T.; Cerny, M. A.; Zhang, X.; Johnson, E. F.; Cashman, J. R. *J. Med. Chem.* **2006**, *49*, 6987−7001.
(40) Guex, N.; Peitsch, M. *Electrophoresis* **1997**, *18*, 2714−2723.
(41) Chen, V. B.; Arendall, W. B., III; Headd, J. J.; Keedy, D. A.; Immormino, R. M.; Kapral, G. J.; Murray, L. W.; Richardson, J. S.; Richardson, D. C. *Acta Crystallogr., Sect. D: Biol. Crystallogr.* **2010**, *66*, 12−21.
(42) Davis, E. A. *Nucleic Acids Res.* **2007**, *35*, W375−W383.
(43) Rydberg, P.; Olsen, L.; Norrby, P.-O.; Ryde, U. *J. Chem. Theory Comput.* **2007**, *3*, 1765−1773.
(44) Frisch, M. J.; Trucks, G. W.; Schlegel, H. B.; Scuseria, G. E.; Robb, M. A.; Cheeseman, J. R.; Montgomery Jr, J. A.; Vreven, T.; Kudin, K. N.; Burant, J. C.; et al.; *Gaussian03*; Gaussian Inc.: Wallingford, CT, 2004.
(45) Gilson, M.; Sharp, K.; Honig, B. *J. Comput. Chem.* **1987**, *9*, 327−335.
(46) Wang, J.; Wang, W.; Kollman, P.; Case, D. *J. Mol. Graph. Model.* **2006**, *25*, 247−260case.
(47) Case, D.; Darden, T.; Cheatham, I., TE; Simmerling, C.; Wang, J.; Duke, R.; Luo, R.; Merz, K.; Pearlman, D.; Crowley, M.; et al. *Amber 9*; University of California: San Francisco, 2006.
(48) Thompson, M. *ACS meeting*; American Chemical Society: Washington, DC, 2004; Vol. *172*; pp CINF 42, PA.
(49) Jorgensen, W.; Chandrasekar, J.; Madura, J.; Impey, R.; Klein, M. *J. Phys. Chem.* **1983**, *79*, 926−935.
(50) Svensson, M.; Humbel, S.; Froese, R.; Mastubara, T.; Sieber, S.; Morokuma, K. *J. Phys. Chem.* **1996**, *100*, 19357−19363.
(51) Lee, C.; Yang, W.; Parr, R. *Phys. Rev. B* **1988**, *37*, 785−789.
(52) Becke, A. D. *J. Chem. Phys.* **1992**, *96*, 2155−2160.
(53) Becke, A. D. *J. Chem. Phys.* **1992**, *97*, 9173−9177.
(54) Becke, A. D. *J. Phys. Chem.* **1993**, *98*, 5648−5652.
(55) Stephens, P.; Devlin, F.; Chabalowski, C.; Frisch, M. J. *J. Phys. Chem.* **1994**, *98*, 11623−11627.
(56) Hay, P. J.; Wadt, W. R. *J. Chem. Phys.* **1985**, *82*, 299−310.
(57) Friesner, R.; Murphy, R.; Beachy, M.; Ringnalda, M.; Pollard, W.; Dunietz, B.; Cao, Y. *J. Phys. Chem. A* **1999**, *103*, 1913−1928.
(58) Cornell, W.; Cieplak, P.; Bayly, C.; Gould, I.; Merz, K. J.; Ferguson, D.; Spellmeyer, D.; Fox, T.; Caldwell, J.; Kollman, P. *J. Am. Chem. Soc.* **1995**, *117*, 5179−5197.
(59) Frisch, M. J.; Trucks, G. W.; Schlegel, H. B.; Scuseria, G. E.; Robb, M. A.; Cheeseman, J. R.; Scalmani, G.; Barone, V.; Mennucci, B.; Petersson, G. A.; et al.; *Gaussian09*; Gaussian, Inc.: Wallingford, CT, 2009.
(60) Fukui, K. *Acc. Chem. Res.* **1981**, *14*, 363−368.
(61) Shaik, S.; Cohen, S.; de Visser, S.; Sharma, P.; Kumar, D.; Kozuch, S.; Ogliaro, F.; Danovich, D. *Eur. J. Inorg. Chem.* **2004**, 207−226.
(62) Vreven, T.; Byun, K. S.; Komáromi, I.; Dapprich, S.; Montgomery, J. A.; Morokuma, K.; Frisch, M. J. *J. Chem. Theory Comput.* **2006**, *2*, 815−826.
(63) Anisimov, V.; Paneth, P. *J. Math. Chem.* **1999**, *26*, 75−86.
(64) Melander, L.; Saunders, W. H. In *Reaction Rates of Isotopic Molecules*; John Wiley & Sons: New York, 1982; pp 283−307.
(65) Wigner, E. *Z. Phys. Chem. B* **1932**, *19*, 203−216.
(66) Martin, D. E.; Robertson, E. G.; MacLellan, J. G.; Godfrey, P. D.; Thompson, C. D.; Morrison, R. J. S. *J. Am. Chem. Soc.* **2009**, *131*, 2638−2646.
(67) Graton, J.; Berthelot, M.; Gal, J. F.; Girard, S.; Laurence, C.; Lebreton, J.; Le Questel, J. Y.; Maria, P. C.; Naus, P. *J. Am. Chem. Soc.* **2002**, *124*, 10552−10562.
(68) Graton, J.; van Mourik, T.; Price, S. L. *J. Am. Chem. Soc.* **2003**, *125*, 5988−5997.
(69) DeLano, W.; DeLano Scientific LLC: Palo Alto, CA, 2002.
(70) Yano, J.; Hsu, M.; Griffin, K.; Stout, C.; Johnson, E. *Nat. Struct. Mol. Biol.* **2005**, *12*, 822−823.
(71) Scott, E. *Drug Metab. Dispos.* **2009**, *37*, 1319−1327.
(72) Feher, M.; Williams, C. I. *J. Chem. Inf. Model.* **2012**, *52*, 724−738.
(73) Kwiecień, R. A.; Molinié, R.; Paneth, P.; Silvestre, V.; Lebreton, J.; Robins, R. J. *Arch. Biochem. Biophys.* **2011**, *510*, 35−41.
(74) Kwiecień, R. A.; Kosieradzka, K.; Le Questel, J.-Y.; Lebreton, J.; Gentil, E.; Delaforge, M.; Paneth, P.; Robins, R. J. *ChemCatChem* **2012**, *4*, 530−539.
(75) Kumar, D.; Altun, A.; Shaik, S.; Thiel, W. *Faraday Discuss.* **2011**, *148*, 373−383.